

NLO forward-backward charge asymmetries in $p\bar{p} \rightarrow l^- l^+ j$ production at large hadron colliders

F. del Aguila^a, Ll. Ametller^b and R. Pittau^{a 1}

^a *Departamento de Física Teórica y del Cosmos and Centro Andaluz de Física de Partículas Elementales (CAFPE), Universidad de Granada, E-18071 Granada, Spain.*

^b *Departament de Física i Enginyeria Nuclear, Universitat Politècnica de Catalunya, E-08034 Barcelona, Spain.*

Abstract

We consider the next-to-leading order corrections, $\mathcal{O}(\alpha_s)$, to forward-backward charge asymmetries for lepton-pair production in association with a large transverse momentum jet at large hadron colliders. We find that the leading order results are essentially confirmed. Although experimentally challenging and in practice with large backgrounds, these observables could provide a new determination of the weak mixing angle $\sin^2 \theta_{\text{eff}}^{\text{lept}}(M_Z^2)$ with a statistical precision for each lepton flavour of $\sim 10^{-3}$ (7×10^{-3}) at LHC (Tevatron), and if b jets are identified, of the b quark Z asymmetry A_{FB}^b with a statistical precision of $\sim 2 \times 10^{-3}$ (4×10^{-2}) at LHC (Tevatron).

PACS: 13.85.-t, 14.70.-e

Keywords: Hadron-induced high- and super-high-energy interactions, Gauge bosons.

¹ On leave of absence from Dipartimento di Fisica Teorica, Torino and INFN Sezione di Torino, Italy.

INTRODUCTION

The large cross sections for gauge boson production at the Fermilab Tevatron and the CERN Large Hadron Collider (LHC) might give a chance to determine the electroweak parameters with high precision [1, 2]. In practice, the experimental challenge is very demanding, but at any rate pursuing such measurements will help to disentangle the strong physics contributing to the different processes. In this paper we calculate the forward-backward charge asymmetries of lepton pairs in events with a large transverse momentum jet $p\bar{p} \rightarrow Z, \gamma^* + j \rightarrow e^-e^+ + j$ ² at next-to-leading order (NLO), $\mathcal{O}(\alpha_s)$ corrections. We make use of the Monte Carlo program MCFM v4.1 [3], which includes the necessary processes at this order, and of ALPGEN [4]. The particularly interesting case of a final b jet is discussed in detail. We find that the leading order (LO) predictions [5] are essentially confirmed.

Electron-positron pair production $p\bar{p} \rightarrow Z, \gamma^* \rightarrow e^-e^+$ has a large cross section at large hadron colliders, and as it is sensitive to the presence of vector and axial-vector fermion couplings to neutral gauge bosons, in principle allows for their precise measurement. A prime example is the determination of the effective weak mixing angle $\sin^2 \theta_{\text{eff}}^{\text{lept}}$, that enters in their definition, the optimum observable being the forward-backward charge asymmetry of the lepton pairs A_{FB} [6, 7]. Indeed, the tree level Drell-Yan³ parton process $q\bar{q} \rightarrow Z, \gamma^* \rightarrow e^-e^+$ gives an asymmetric polar angle electron distribution relative to the initial quark, which also depends on the lepton pair invariant mass $M_{e^-e^+}$.

At the Fermilab Tevatron Run I the Collider Detector at Fermilab (CDF) reported an asymmetry A_{FB} at the Z peak of 0.07 ± 0.02 [9], in agreement with the Standard Model (SM) prediction. A new measurement of neutral gauge boson production in $p\bar{p}$ collisions at the upgraded Run II Fermilab Tevatron operated at $\sqrt{s} = 1.96$ TeV has been recently presented by CDF, giving, at the Z peak, $A_{\text{FB}} = 0.07 \pm 0.03$, the statistical error being large because only an integrated luminosity of 72 pb^{-1} has been analysed [10], less than a tenth of the luminosity collected so far.⁴ A fit to these data where the quark and electron couplings to

² Throughout the paper we will explicitly refer to the $e^-e^+(+j)$ decay channel. The same analysis applies to $l^-l^+ + j$ production with $l = \mu$.

³ A list of Drell-Yan cross section measurements at Tevatron run I and II is given in Ref. [8].

⁴ In Run I the asymmetry found for the last bin, $M_{e^-e^+} \in [300, 600] \text{ GeV}$, deviated from the SM prediction [9], what is not confirmed by Run II [10].

the Z boson are expressed as a function of $\sin^2 \theta_{\text{eff}}^{\text{lept}}$ gives $\sin^2 \theta_{\text{eff}}^{\text{lept}} = 0.2238 \pm 0.0040 \pm 0.0030$, where the errors stand for statistics and systematics, respectively. This is far away from the estimate of the expected statistical precision ~ 0.0005 to be reached at Run II with an integrated luminosity of 10 fb^{-1} [11]. Even if the experiment is well understood [10] and the theoretical calculations not ambiguous, it seems very hard to get rid of systematic uncertainties to the required level. In the following with a more exclusive process we will need a more demanding experimental performance. But we will stay on the very optimistic side, emphasizing what we may learn if we were only limited by statistics. At LHC with an integrated luminosity of 100 fb^{-1} the weak mixing angle precision would be hopefully further improved by a factor ~ 3 . This would be comparable to the current global fit precision, 0.00016, but for instance a factor ~ 2 better than the effective weak mixing angle precision obtained from the bottom forward-backward asymmetry at LEP and SLD, 0.00029 [12].

The associated production of a neutral gauge boson $V = Z, \gamma^*$ and a jet j has also a large cross section, especially at LHC, and can also allow for a precise determination of $\sin^2 \theta_{\text{eff}}^{\text{lept}}$. This NLO correction to V production is a genuine new process when we require the detection of the extra jet. In particular, gluons can be also initial states, and the large gluon content of the proton at high energy tends to increase the Vj production cross sections, although they stay almost one order of magnitude smaller than the corresponding V cross sections. In Table II of the section that collects our numerical results we gather the different LO and NLO contributions to $V(\rightarrow e^-e^+)j$ production at Tevatron, to be compared with the inclusive LO and NLO $V \rightarrow e^-e^+$ cross section for the same cuts, 127 and 158 pb, respectively. At LHC we find for e^-e^+ production 685 and 745 pb, respectively, to be compared to the e^-e^+j cross section, 53 and 57 pb, in Table II below. All the calculations throughout the paper have been performed with MCFM v4.1, and with ALPGEN when necessary. They provide a good description of these processes at hadron colliders. For instance, the prediction at Tevatron for the ratio of the inclusive cross section for $p\bar{p} \rightarrow V(\bar{b})$ to $p\bar{p} \rightarrow Vj$ production is, according to the results in Table II below, 0.020 to NLO ⁵ (0.0096 to LO [5]). ⁶ This has to be compared to the recent measurement of this ratio with the D0 detector 0.023 ± 0.005 [13], obtained with a similar, but not identical, set of cuts.

⁵ We neglect in this estimate the small fraction of events where b and \bar{b} combine into the same jet.

⁶ In apparent agreement with the NLO prediction 0.018 ± 0.004 by J.M. Campbell and Willenbrock quoted in Ref. [13].

As pointed out in Ref. [5] the forward-backward charge asymmetry of the lepton pairs can be measured in neutral gauge boson production with an accompanying jet either relative to a direction fixed by the initial state $A_{\text{FB}}^{\text{CS}}$ as in the inclusive neutral gauge boson production (Drell-Yan case), or relative to the final jet direction A_{FB}^j . The former is adapted to obtain the asymmetry from $q\bar{q}$ events, and the latter from $g^{(\bar{q})}$ ones. Both asymmetries give similar precision for $\sin^2 \theta_{\text{eff}}^{\text{lept}}$ at LHC but not at Tevatron, where the precision for $A_{\text{FB}}^{\text{CS}}$ is almost one order of magnitude higher. However, in principle A_{FB}^j also allows for the measurement of flavour asymmetries. Thus, if we require the final jet to be a b quark, we can make a new measurement of A_{FB}^b . This is especially interesting given its observed deviation at the Z pole from the SM prediction, 3σ [12]. However, to approach a similar precision will be a very demanding experimental challenge because we have not only to identify the heavy quark but to measure its charge. Being very optimistic the corresponding effective weak mixing angle precision to be in principle expected at LHC, $\sim 10^{-3}$, is already lower than the one reported by LEP and SLD, 2.9×10^{-4} , but similar to the difference between the central values resulting from A_{FB}^b at the Z pole and the global fit to all data [12].

In the following we study the LHC and the Tevatron potentials in turn. First, we review the LO contributions to $p\bar{p}^{(\bar{q})} \rightarrow Vj$ production and introduce the different asymmetries. Afterward we discuss the NLO corrections, paying special attention to the case of a final b jet. Finally, we present the numerical results and draw our conclusions.

LO PROCESSES AND FORWARD-BACKWARD CHARGE ASYMMETRIES

Let us thus compare the processes

$$p\bar{p}^{(\bar{q})} \rightarrow Z, \gamma^* \rightarrow e^- e^+ \quad (1)$$

and

$$p\bar{p}^{(\bar{q})} \rightarrow Z, \gamma^* + j \rightarrow e^- e^+ + j \quad (2)$$

at LO and define the different forward-backward asymmetries we are interested in. Fig. 1 shows the LO diagram contributing to the Drell-Yan process in Eq. 1. In the absence of gluonic radiation the transverse momentum of the exchanged vector boson is zero. Therefore, one must, for instance, expect that the direction of the initial quark state and the final e^-

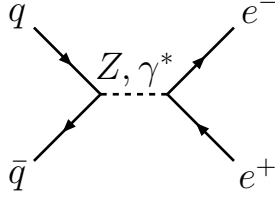


FIG. 1: LO $q\bar{q}$ contribution to the Drell-Yan process in Eq. 1.

are correlated. When the initial quark line emits gluons, such correlations, although still present, tend to diminish because of the transverse momentum p_t acquired by the e^-e^+ system. If one of those additional gluons is hard enough and is emitted in the central region of the detector, it gives rise to an extra jet resulting into the process in Eq. 2. However, allowing for an extra jet obliges to consider new subprocess initiated by a gluon and a(n) (anti)quark. We show in Fig. 2 the relevant tree level diagrams in the simple case $j = b$. In diagram (b) the decay products of the Z, γ^* system know very little about the direction

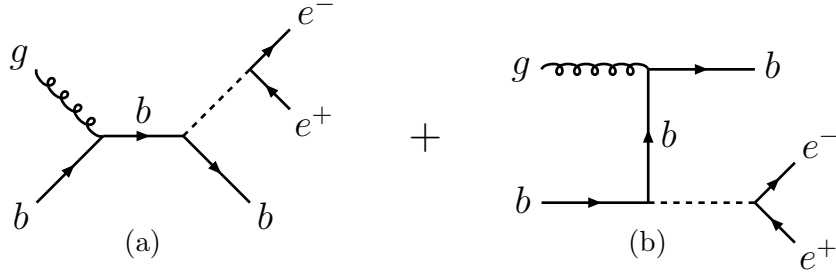


FIG. 2: LO gb contributions to the process in Eq. 2 for $j = b$.

of the final state b , because of the initial state gluon that also connects to the b fermionic line. Instead, in diagram (a), the p_t of the b quark exchanged in the s -channel is zero, therefore one expects correlations between the final state leptons and the direction of the b -jet ⁷ [5]. An optimal observable to quantify such correlations for the process of Eq. 2 is a forward-backward asymmetry:

$$A_{\text{FB}} = \frac{F - B}{F + B}, \quad (3)$$

with

$$F = \int_0^1 \frac{d\sigma}{d\cos\theta} d\cos\theta, \quad B = \int_{-1}^0 \frac{d\sigma}{d\cos\theta} d\cos\theta.$$

⁷ Analogous considerations also hold in the general case with $j \neq b$.

One can consider two possible angles:

$$\cos \theta_{\text{CS}} = \frac{2(p_z^{e^-} E^{e^+} - p_z^{e^+} E^{e^-})}{\sqrt{(p^{e^-} + p^{e^+})^2} \sqrt{(p^{e^-} + p^{e^+})^2 + (p_T^{e^-} + p_T^{e^+})^2}},$$

$$\cos \theta_j = \frac{(p^{e^-} - p^{e^+}) \cdot p^j}{(p^{e^-} + p^{e^+}) \cdot p^j},$$

where the four-momenta are measured in the laboratory frame and $p_T^\mu \equiv (0, p_x, p_y, 0)$. The Collins-Soper angle [14] θ_{CS} is, on average, the angle between e^- and the initial quark direction, while θ_j is the angle between e^- and the direction opposite to the jet in the e^-e^+ rest frame [5]. From the previous discussion it should be clear that the former choice is adapted to the $q\bar{q}$ collisions and the latter to the $g(\bar{q})$ ones.

Different asymmetries can be defined, according to the scheme given in Table I. A

Collider	Asymmetry	Definition
$p\bar{p}$	$A_{\text{FB}}^{\text{CS}}$	$\cos \theta = \cos \theta_{\text{CS}}$
pp	$A_{\text{FB}}^{\text{CS}}$	$\cos \theta = \cos \theta_{\text{CS}} \times \frac{ p_z^{e^+} + p_z^{e^-} + p_z^j }{p_z^{e^+} + p_z^{e^-} + p_z^j}$
$p\bar{p}$	A_{FB}^j	$\cos \theta = \cos \theta_j \times \frac{ p_z^{e^+} + p_z^{e^-} + p_z^j }{p_z^{e^+} + p_z^{e^-} + p_z^j}$
pp	A_{FB}^j	$\cos \theta = \cos \theta_j$
$p\bar{p}$	A_{FB}^b	$\cos \theta = \cos \theta_j \times (-\text{sign}(Q_b))$
pp	A_{FB}^b	$\cos \theta = \cos \theta_j \times (-\text{sign}(Q_b))$

TABLE I: The definitions of the various asymmetries at the pp and $p\bar{p}$ colliders.

comment is in order, with respect to the phases appearing in the Table. In pp colliders the quark direction is fixed by the rapidity of the jet plus the lepton pair. This implies defining $\cos \theta_{\text{CS}}$ with an extra sign factor $\frac{|p_z^{e^-} + p_z^{e^+} + p_z^j|}{p_z^{e^-} + p_z^{e^+} + p_z^j}$, as in the second line of Table I. On the other hand, in $p\bar{p}$ colliders there are produced as many quarks as antiquarks and A_{FB}^j vanishes unless some difference is made between them. Hence, $\cos \theta$ is defined with an extra sign factor $\frac{|p_z|}{p_z}$, $p = p^{e^-} + p^{e^+} + p^j$, which corresponds to assume that the largest rapidity parton is a (anti)quark if it is along the (anti)proton direction. This explains the factor in the third line of Table I. Finally, because both in pp and $p\bar{p}$ colliders are produced as many b as \bar{b} , in order to obtain A_{FB}^b one must use $\cos \theta_j$ multiplied by a $+(-)$ sign for b (anti)quarks, $-\text{sign}(Q_b)$ with Q_b the b charge. In practice this means detecting the charge of the produced b jet.

Such asymmetries have been studied in detail, at LO, in Ref. [5]. What is important to realize is that, in order to get reliable predictions, a priori small additional contributions must be carefully taken into account. Let us study, in particular, the effect of including radiative $\mathcal{O}(\alpha_s)$, NLO, corrections.

NLO CONTRIBUTIONS

In the following we discuss all contributions necessary to compute the process in Eq. 2 at the NLO. The described structure is implemented in the MCFM code, that we used as it is in the case $j \neq b$. However, as already pointed out, the computation of A_{FB}^b requires disentangling b from \bar{b} final states. In MCFM this selection is not possible on an event by event basis, because b and \bar{b} contributions are summed up. Therefore, we modified the code to take this into account. In addition, we included part of the remaining real NLO contribution with the help of ALPGEN. We find convenient to list the different contributions in the following, for the case $j = b$, because this will allow us to discuss their relative size. Analogous considerations apply to the general case.

The virtual contributions are drawn in Fig. 3, together with the definition of all the graphical symbols and conventions used. In particular, we omit drawing explicitly the decay of the Z, γ^* system, but we always understand $Z, \gamma^* \rightarrow e^- e^+$, and the blob stands for the sum of all possible contributing Feynman diagrams. For the case at hand, it means exchanging a virtual gluon in all possible ways in the two diagrams of Fig. 2.

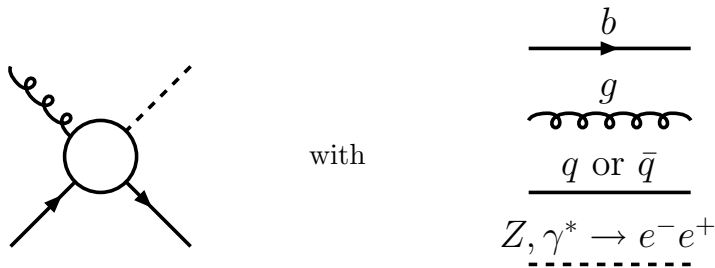


FIG. 3: NLO virtual gb contributions.

The real contributions are given in Fig. 4. The shorter lines on the right part of the drawings means that the corresponding outgoing partons are not seen because they are too soft or too collinear to the ingoing or outgoing b quark, therefore also leading to a final state

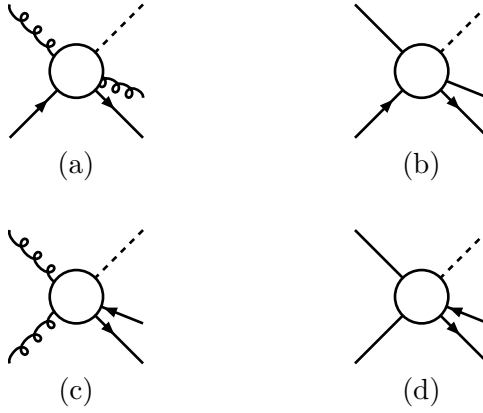


FIG. 4: NLO real gb (a), $\bar{q}b$ (b), gg (c), $q\bar{q}$ (d) contributions.

formed by an e^-e^+ pair plus a jet containing a b quark. The NLO fully differential cross section $d\sigma^{\text{NLO}}$ is given by

$$d\sigma^{\text{NLO}} = \sum_{i,j} \int_0^1 dx_1 \int_0^1 dx_2 f_i^{\text{NLO}}(x_1) f_j^{\text{NLO}}(x_2) d\hat{\sigma}_{ij}^{\text{NLO}}, \quad (4)$$

$$i, j = g, b, q, \bar{q}$$

where $f_i^{\text{NLO}}(x)$ is the parton density, evolved at the NLO, relative to the i^{th} initial state particle, carrying a fraction x of the proton (or antiproton) longitudinal momentum

$$f_i^{\text{NLO}}(x) = f_i^{(0)}(x) + \alpha_s f_i^{(1)}(x), \quad (5)$$

and $d\hat{\sigma}_{ij}^{\text{NLO}}$ are the differential cross sections corresponding to the subprocesses given in Figs. 3 and 4 computed at the one loop accuracy in QCD

$$d\hat{\sigma}_{ij}^{\text{NLO}} = d\hat{\sigma}_{ij}^{(0)} + \alpha_s d\hat{\sigma}_{ij}^{(1)}. \quad (6)$$

The separation between virtual and real contributions in $d\hat{\sigma}_{ij}^{(1)}$ is performed in MCFM with the help of a Dipole Formalism [15].

It is worth discussing the relative size of all the terms appearing in Eq. 4. Setting the scale of the hard scattering to $\mu = M_Z$, the distribution function $f_b^{(0)}(x)$ intrinsically sums up all contributions of the order $\alpha_s^k L^k$ [16], where $L = \ln(\mu/m_b)$ is the large collinear logarithm associated to the fact that $f_b^{(0)}(x)$ describes an exactly collinear gluon splitting $g \rightarrow b\bar{b}$. Therefore, the leading order term

$$d\sigma^{(0)} = \int_0^1 dx_1 \int_0^1 dx_2 f_g^{(0)}(x_1) f_b^{(0)}(x_2) d\hat{\sigma}_{gb}^{(0)} + (g \leftrightarrow b), \quad (7)$$

coming from the diagrams in Fig. 2 contains all possible $\alpha_s^k L^k$ contributions

$$d\sigma^{(0)} = \sum_{k=1}^{\infty} c_k \alpha_s^k L^k. \quad (8)$$

Including the diagrams in Figs. 3, 4(a) and 4(b) takes into account all corrections order $\alpha_s^{(k+1)} L^k$, because the corresponding subprocesses multiply $f_b^{(0)}(x)$ in Eq. 4. The corrections given in Fig. 4(c) correspond to the contributions $\mathcal{O}(\alpha_s)$ or $\mathcal{O}(\alpha_s L)$, depending whether the final state \bar{b} is or is not collinear to one of the initial state gluons⁸. They correct the leading order picture implicit in Eq. 7 of exactly collinearly produced b : now the initial state b can acquire a p_t . However, as discussed, *all* collinear contributions are already included in the LO process, in particular the $k = 1$ term in Eq. 8, therefore we are facing an apparent double counting. The key for understanding that this is not the case is noticing that other contributions are present in Eq. 4, that correspond to the evolution of the parton densities

$$\alpha_s \left(f_g^{(1)}(x_1) f_b^{(0)}(x_2) + f_g^{(0)}(x_1) f_b^{(1)}(x_2) \right) d\hat{\sigma}_{gb}^{(0)} + (g \leftrightarrow b). \quad (9)$$

Their effect is, among others, subtracting the $c_1 \alpha_s L$ term from the LO contribution in Eq. 8, so that adding the corrections of Fig. 4(c), does not imply double counting. The structure described so far is implemented in MCFM, that we had to modify in order to disentangle b and \bar{b} production, which is necessary, in our case, for computing A_{FB}^b .

Finally, we computed the pure $\mathcal{O}(\alpha_s)$ corrections in Fig. 4(d) with the help of ALPGEN. In the next section we discuss our numerical findings.

NUMERICAL RESULTS

We present our numerical results for $e^- e^+ j$ and $e^- e^+ b$ at LHC and Tevatron in turn. Our simulation of the set up at LHC (Tevatron) is as follows

$$p_t^e > 20 \text{ GeV}, \quad p_t^j > 50 \text{ (30) GeV}, \\ |\eta^{e,j}| < 2.5, \quad \Delta R_{e,j} > 0.4.$$

For muon pairs the main difference would be the pseudorapidity coverage [17, 18]. We use the `cteq6l1` (`cteq6m`) parton distributions at LO (NLO) [19]. The effect of smearing the

⁸ Note that such collinear or almost collinear configurations contribute to the exclusive process we are studying when the final state \bar{b} is lost in the forward or backward regions of the detector.

lepton and jet energies has been studied at LO and found to be negligible [5], therefore we do not include it here. On the other hand, the dominant background processes are expected to be the same as for Drell-Yan production, namely, jets misidentified as e^\pm , and $p\bar{p}^{(\pm)} \rightarrow W^+W^-j \rightarrow e^+e^-\nu_e\bar{\nu}_ej$. They are understood experimentally, at least at Tevatron, and can be considered under control [10]. The LO and NLO production rates at LHC and Tevatron are given in Table II. In Figs. 5 (6) we show the corresponding charge asymmetries,

Contributing process	LHC		Tevatron	
	LO	NLO	LO	NLO
$g\bar{q}^{(\pm)} \rightarrow Vj(j)$	44.3	53.4	3.40	4.77
$q\bar{q} \rightarrow Vj(j)$	8.4	} 3.7	4.61	} 2.76
$\bar{q}^{(\pm)}q^{(\pm)} \rightarrow Vj(j)$	—		—	
$gg \rightarrow Vj(j)$	—		—	
Total	52.7	57.1	8.01	7.53
$gb \rightarrow Vb(g)$	1.81	} 1.81	0.038	} 0.049
$gg \rightarrow Vb(\bar{b})$	—		—	
$\bar{q}^{(\pm)}b \rightarrow Vb(\bar{q}^{(\pm)})$	—		—	
$q\bar{q} \rightarrow Vb(\bar{b})$	—	0.06	—	0.025
Total	1.81	1.87	0.038	0.074

TABLE II: Estimates for the e^-e^+j and e^-e^+b cross sections at LHC ($\sqrt{s} = 14$ TeV) and Tevatron ($\sqrt{s} = 1.96$ TeV) in pb. The jet transverse momenta are required to be larger than 50 (30) GeV at LHC (Tevatron) and all pseudorapidities $|\eta|$ smaller than 2.5. The p_t of the leptons is larger than 20 GeV. The separations in the pseudorapidity-azimuthal angle plane satisfy $\Delta R > 0.4$ and $M_{e^-e^+}$ is within the range [75, 105] GeV. $\bar{q}^{(\pm)}$ means summing over q and \bar{q} contributions.

$A_{\text{FB}}^{\text{CS}}$ relative to the initial parton and A_{FB}^j , A_{FB}^b relative to the final jet.

The effect of the $\mathcal{O}(\alpha_s)$ corrections is moderate for $A_{\text{FB}}^{\text{CS}}$ and A_{FB}^j , but sizable for A_{FB}^b , especially at Tevatron. This is basically due to the genuine new higher order process $q\bar{q} \rightarrow Vb(\bar{b})$ in Fig. 4(d), that tends to wash out the asymmetry which is mainly associated to the (a) contribution in Fig. 2. This change is more pronounced at Tevatron energies, where the $q\bar{q}$ content of the (anti)proton is larger (see Table II). In all cases the asymmetries at NLO

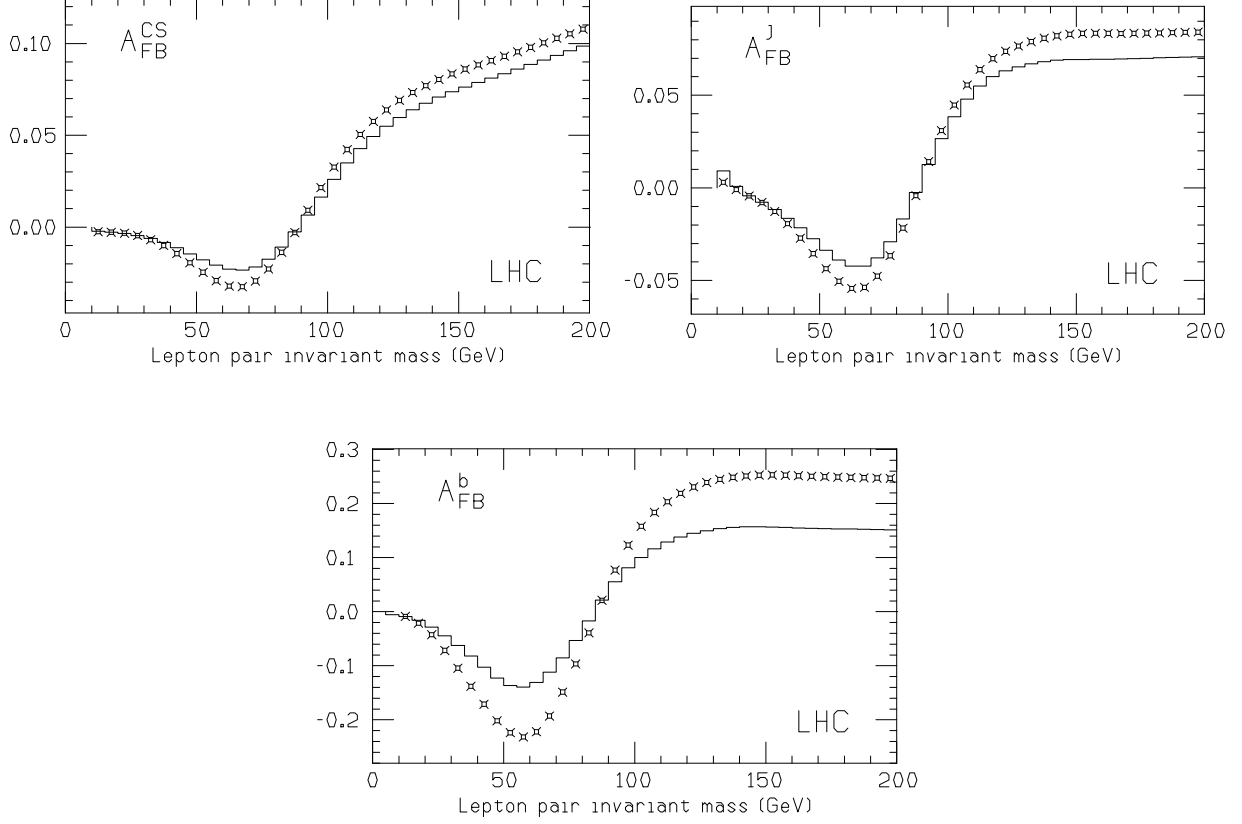


FIG. 5: NLO (solid histogram) and LO (points) asymmetries at LHC.

diminish, except for A_{FB}^j at Tevatron where this asymmetry is smaller.

Near the Z pole, $M_{e^-e^+} \sim M_Z$, the asymmetries can be approximated by [6]

$$A = b(a - \sin^2 \theta_{\text{eff}}^{\text{lept}}(M_Z^2)), \quad (10)$$

translating then their measurement into a precise determination of $\sin^2 \theta_{\text{eff}}^{\text{lept}}(M_Z^2)$. In Table III we collect the asymmetry estimates, their statistical precision, the cross sections and the precision reach $\delta \sin^2 \theta_{\text{eff}}^{\text{lept}}$ of LHC and Tevatron for $M_{e^-e^+}$ in the range $[75, 105]$ GeV, by assuming an integrated Luminosity L of 100 (10) fb^{-1} at LHC (Tevatron). In the Table we assumed a b -tagging efficiency ϵ of 100 %, no contamination ω and, in particular, no charge misidentification. The statistical precisions δA and $\delta \sin^2 \theta_{\text{eff}}^{\text{lept}}$ are proportional to $\epsilon^{-\frac{1}{2}}$, and the asymmetries A to $1 - 2\omega$. Therefore the contamination multiplies $\delta \sin^2 \theta_{\text{eff}}^{\text{lept}}$ by $(1 - 2\omega)^{-1}$. Thus, if we only consider semileptonic b decays, implying $\epsilon \sim 0.1$ and $\omega \sim 0$, δA and $\delta \sin^2 \theta_{\text{eff}}^{\text{lept}}$ increase by a factor ~ 3 . In practice we must try to maximize the quality factor $Q = \epsilon(1 - 2\omega)^2$ [20]. Although the exact value of ω can only be inferred

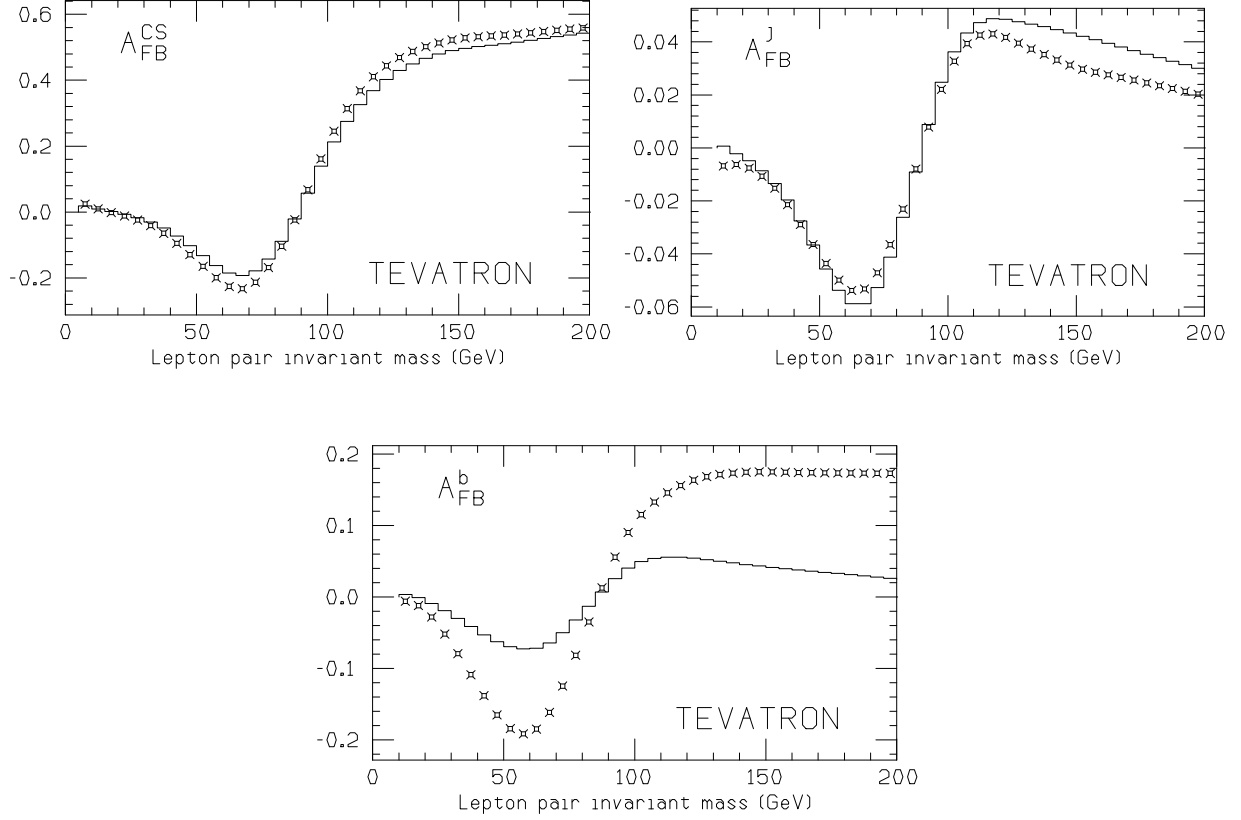


FIG. 6: NLO (solid histogram) and LO (points) asymmetries at Tevatron.

from dedicated experimental studies, it is instructive to have an idea of its typical size. This can be achieved by comparing the charge separation δ_b , measured at LEP using a jet charge technique, with the value $2Q_b = -\frac{2}{3}$ one would get if the b quark could be directly observed [21]. This comparison gives $\omega \sim 0.3$. The statistical precisions given in Table III are certainly optimistic for systematic errors are also sizable. At any rate approaching the quoted precisions will be an experimental challenge.

A second source of uncertainty, that is not accounted for in Table III, is the dependence of the results on the chosen set of parton densities. We investigated it by recomputing asymmetries and statistical precisions using different parton distribution sets in the classes `cteq` and `mrst` [22]. By doing so, variations of the asymmetries of the order of 10% can be easily observed in the range $75 \text{ GeV} < M_{e^-e^+} < 105 \text{ GeV}$, both at Tevatron and LHC, while the statistical precisions are not significantly affected. This rather important dependence on the parton densities can be considered as an extra handle provided by the asymmetry measurements in constraining the parton distribution functions. Conversely, with a more

LO NLO	$\sigma(\text{pb})$		A_{FB}	δA_{FB}	$\delta \sin^2 \theta_{\text{eff}}^{\text{lept}}$
LHC	$\sigma^{Vj} = 53$	$A_{\text{FB}}^{\text{CS}}$	8.7×10^{-3}	4.4×10^{-4}	1.3×10^{-3}
	57		6.8×10^{-3}	4.2×10^{-4}	1.3×10^{-3}
		A_{FB}^j	1.2×10^{-2}	4.4×10^{-4}	8.8×10^{-4}
			1.1×10^{-2}	4.2×10^{-4}	1.1×10^{-3}
	$\sigma^{Vb} = 1.8$	A_{FB}^b	7.5×10^{-2}	2.3×10^{-3}	8.7×10^{-4}
	1.9		4.9×10^{-2}	2.3×10^{-3}	1.4×10^{-3}
Tevatron	$\sigma^{Vj} = 8.0$	$A_{\text{FB}}^{\text{CS}}$	6.4×10^{-2}	3.5×10^{-3}	1.4×10^{-3}
	7.5		5.5×10^{-2}	3.6×10^{-3}	1.7×10^{-3}
		A_{FB}^j	9.9×10^{-3}	3.5×10^{-3}	8.1×10^{-3}
			1.1×10^{-2}	3.6×10^{-3}	7.2×10^{-3}
	$\sigma^{Vb} = 0.04$	A_{FB}^b	5.5×10^{-2}	5.1×10^{-2}	2.5×10^{-2}
	0.07		2.7×10^{-2}	3.7×10^{-2}	4.7×10^{-2}

TABLE III: Estimates for the e^-e^+j and e^-e^+b cross sections and asymmetries defined in the text with $M_{e^-e^+}$ in the range $[75, 105]$ GeV. The first row of each entry is the LO result, while the second one refers to the NLO. The integrated luminosity as well as the cuts can be found in the text. The statistical precisions are also given, to be compared with the current effective weak mixing angle uncertainties at LEP and SLD from asymmetries only 1.6×10^{-4} , and from A_{FB}^b at the Z pole 2.9×10^{-4} [12].

precise knowledge of them, the charge asymmetries can be used for precision measurements.

CONCLUSIONS

In summary, the large Vj production cross section at hadron colliders and the possibility of measuring the lepton asymmetries relative to the final jet allow for a precise determination of the effective electroweak mixing angle. We have evaluated them to NLO, confirming to a large extent the LO results. If there is an efficient b -tagging and charge identification, these events with a b jet also allow for a new determination of A_{FB}^b . The corresponding statistical precisions are collected in Table III. As in Drell-Yan production [23], these processes can be

also sensitive to new physics for large M_{e-e^+} , especially to new gauge bosons.

ACKNOWLEDGMENTS

We thank A. Bueno, J.M. Campbell and T. Rodrigo for useful comments. This work was supported in part by MCYT under contract FPA2003-09298-C02-01 and by Junta de Andalucía group FQM 101, and by MIUR under contract 2004021808_009.

-
- [1] R. Brock *et al.*, in Proceedings of the Workshop on QCD and Weak Boson Physics in Run II, FERMILAB-PUB-00/297 (2000), eds. U. Baur, R.K. Ellis and D. Zeppenfeld, p. 78.
 - [2] S. Haywood *et al.*, in Proceedings of the Workshop on Standard Model Physics (and more) at the LHC, CERN 2000-004 (2000), eds. G. Altarelli and M.L. Mangano, p. 117.
 - [3] J.M. Campbell, R.K. Ellis, Phys. Rev. D **62**, 114012 (2000).
 - [4] M.L. Mangano, M. Moretti, F. Piccinini, R. Pittau, A. Polosa, JHEP **0307**, 001 (2003); for other programs see W. Hollik *et al.*, Acta Phys. Polon. B **35**, 2533 (2004).
 - [5] F. del Aguila, Ll. Ametller and P. Talavera, Phys. Rev. Lett. **89**, 161802 (2002).
 - [6] J.L. Rosner, Phys. Lett. B **221**, 85 (1989).
 - [7] P. Fischer, U. Becker and J. Kirkby, Phys. Lett. B **356**, 404 (1995).
 - [8] T. Affolder *et al.*, Phys. Rev. D **63**, 011101(R) (2001); B. Abbott *et al.*, Phys. Rev. Lett. **82**, 4769 (2000); D. Acosta *et al.*, Phys. Rev. Lett. **94**, 091803 (2005); F. Déliot, hep-ex/0505023.
 - [9] T. Affolder *et al.*, Phys. Rev. Lett. **87**, 131802 (2001); see also F. Abe *et al.*, Phys. Rev. Lett. **77**, 2616 (1996).
 - [10] D. Acosta *et al.*, Phys. Rev. D **71**, 052002 (2005).
 - [11] U. Baur, S. Keller and W.K. Sakumoto, Phys. Rev. D **57**, 199 (1998); U. Baur, O. Brein, W. Hollik, C. Schappacher and D. Wackeroth, Phys. Rev. D **65**, 033007 (2002).
 - [12] Latest results in <http://lepewwg.web.cern.ch/LEPEWWG/>.
 - [13] V.M. Abazov *et al.*, Phys. Rev. Lett. **94**, 161801 (2005).
 - [14] J.C. Collins and D.E. Soper, Phys. Rev. D **16**, 2219 (1977).
 - [15] S. Catani and M.H. Seymour, Phys. Lett. B **378**, 287 (1996) and Nucl. Phys. B **485**, 291 (1997); D. Dicus, T. Stelzer, Z. Sullivan and S. Willenbrock, Phys. Rev. D **59**, 094016 (1999).

- [16] J. Campbell, R.K. Ellis, F. Maltoni, S. Willenbrock, Phys. Rev. D **67**, 095002 (2003) and Phys. Rev. D **69**, 074021 (2004).
- [17] A. Airapetian *et al.*, ATLAS Detector and Physics Performance Technical Design Report, CERN-LHCC 99-14/15, <http://atlasinfo.cern.ch/ATLAS/internal/tdr.html>.
- [18] G. L. Bayatian *et al.*, CMS: the TriDAS Project Technical Design Report, CERN/LHCC 2000-38, <http://cmsdoc.cern.ch/cms/TDR/TRIGGER-public/trigger.html>.
- [19] J. Botts *et al.*, Phys. Lett. B **304**, 159 (1993); H. L. Lai *et al.*, Phys. Rev. D **51**, 4763 (1995); H. L. Lai *et al.*, Phys. Rev. D **55**, 1280 (1997); H. L. Lai *et al.*, Eur. Phys. J. C **12**, 375 (2000); J. Pumplin *et al.*, JHEP **0207**, 012 (2002).
- [20] B. Aubert *et al.*, BABAR Collaboration, Phys. Rev. D **66**, 032003 (2002).
- [21] P. Abreu *et al.*, DELPHI Collaboration, Eur. Phys. J. C **9**, 367 (1999).
- [22] A. D. Martin, R. G. Roberts, W. J. Stirling and R. S. Thorne, Eur. Phys. J. C **4** (1998) 463 and Eur. Phys. J. C **14**, 133 (2000).
- [23] F. del Aguila, M. Quirós and F. Zwirner, Nucl. Phys. B **287**, 419 (1987); J.L. Rosner, Phys. Rev. D **54**, 1078 (1996); T. Affolder *et al.*, Phys. Rev. Lett. **87**, 131802 (2001).